Chapter 1

Nonlinear theory

In this chapter we extended the results of the linear stability analysis to a nonlinear analysis. Through numerical simulations, we suggest that the saturation level of the short-wave aspect ratio depends upon the aspect ratio.

1.1   Set-up

In this section we discuss some numerical tests of the code to verify that the nonlinear results are correctly resolving the smallest scales. In order to do a full DNS, we need to resolve the Kolmogorov scales. The Kolmogorov scale is given by (cite)

$$\eta = \left(\frac{\nu^3}{\epsilon}\right)^3 \tag{1.1}$$

where ϵ is the energy given by

$$\epsilon \sim \frac{U^3}{R} \tag{1.2}$$

where U, R are the characteristic velocity and length respectively. Rewriting the Kolmogorov scale η in terms of the Reynolds number by multiplying by the characteristic length R, which we take to be unity as has been suggested from the linear results, to obtain

$$\eta = \frac{1}{\mathrm{Re}^{3/4}} \tag{1.3}$$

For our simulations, the code separates the horizontal and vertical resolutions, which we denote by Δx and Δz. We want to choose the number of grid points to be such that $\Delta x \approx \Delta z$.

To illustrate, we consider a test case that was run to determine whether or not to use $L = 9$ or $L = 5$ for the box size. Both have been used in practice (cite). Consider a grid with $N \times N \times n$ points, where we have explicitly separated out the horizontal and vertical directions. Because we need to resolve the Kolmogorov scales, we have restrictions on the total number of grid points. We consider the case of $Re = 2000$ and $F_h = 0.2$. The Reynolds number tells us that that the Kolmogorov scale is

$$\eta \sim \frac{1}{Re^{3/4}} \approx 0.003343, \qquad \Delta x \sim \eta \tag{1.4}$$

and thus we want a grid spacing that is approximately 0.003343. Since it is desirable for N to be a power of two, if $N = 1024$ we have that

$$\Delta x = \frac{L}{1024}. \tag{1.5}$$

If $L = 9$ then $\Delta x = 0.00878$ and if $L = 5$ then $\Delta x = 0.00488$. It is clear that it is more desirable to pick $L = 5$ because the grid spacing is closer to the η.

Now we need to set the vertical resolution. It is important that we have the same resolution for the vertical and horizontal so $\Delta x \approx \Delta z$. Since we are interested in investigating the short-wave instability the vertical scale is

$$H \sim \frac{2\pi}{k_z}. \tag{1.6}$$

In this case, the greatest growth rate occurs at the wavenumber $k_z = 20$ and thus the vertical scale is $H = 0.314$. Now setting $\Delta z \approx \Delta x$ for both $L = 5, 9$ we find that for $L = 9$ if $n = 32$ then $\Delta z = 0.00982$ which is close to $\Delta x = 0.00878$. If $L = 5$ then if $n = 64$ then $\Delta z = 0.00491$ which is close to $\Delta x = 0.00488$. Thus to resolve the Kolmogorov scale as much as possible, we should choose $L = 5$ with $N = 1024, n = 64$ over $L = 9$ with $N = 1024, n = 32$. However when the code is actually run $L = 5$ takes roughly 30.8 hours of real time versus 19.5 hours of real time. Additionally, due to the way the code is set-up, $L = 5$ requires twice as many processors as $L = 9$. Additionally, due to the way the code is set-up, $L = 5$ requires twice as many processors as $L = 9$ which requires more resources. Thus a trade-off must be made between running at a higher resolution but taking longer versus running at a lower resolution, in the processing potentially not resolving the Kolmogorov scale, but running faster.
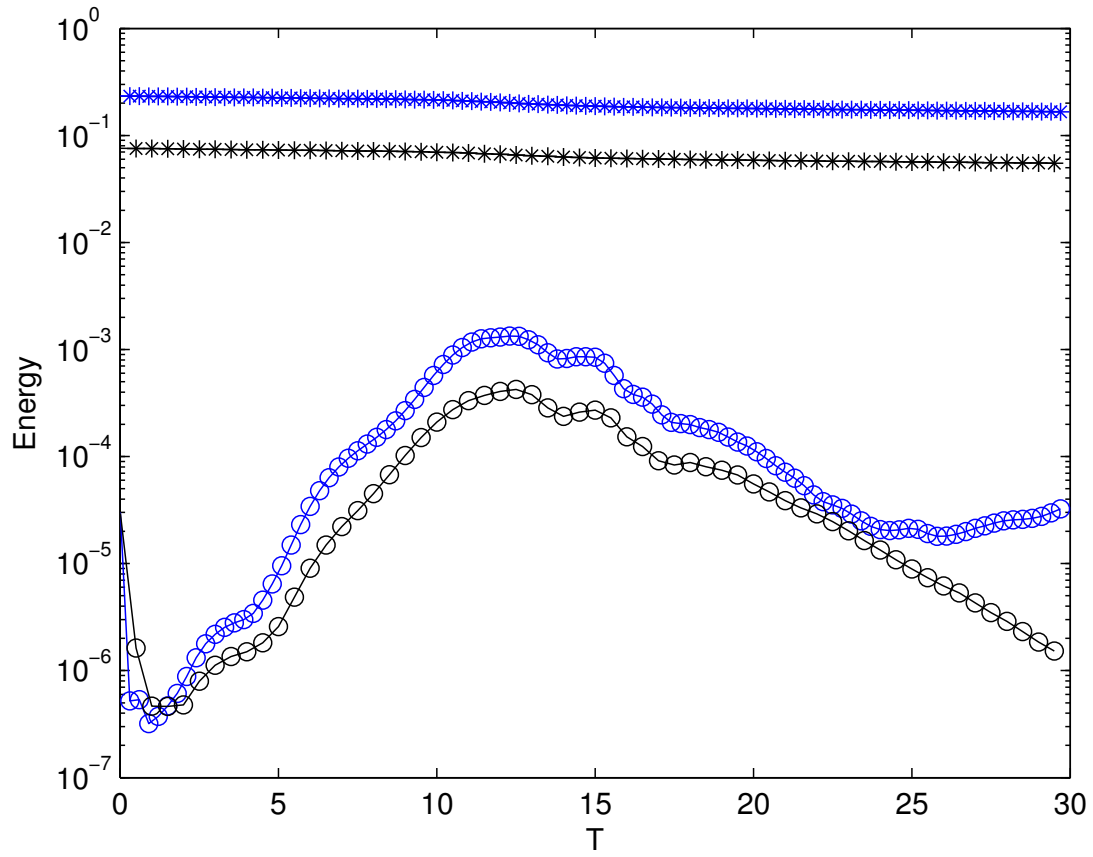
Figure 1.1: Time series of the potential energy (circle) and kinetic energy (star) for $L = 5$ (blue) and $L = 9$ (black).

In Fig. 1.1 we demonstrate two tests run that were done to determine what resolution to use. Qualitatively, both curves are very similar, with the $L = 5$ curves shifted upwards by a constant. This is to be expected because by using a larger domain size, less of the domain is focused on the dipole and thus there is less energy in this dipole. When we decrease the domain size, the dipole takes up a larger percentage of the grid and thus has a larger energy.

When we compute the growth rates and saturation levels, they are in close agreement. Thus we choose $L = 9$ and $n = 32$ for our simulations despite not completely resolving the Kolmogorov scale. Our time step $\Delta = 5.0 \times 10^{-4}$. Each run was initialised with a random density sinusoidal perturbation with $\epsilon = 0.01$.

1.2 Results

The nonlinear evolution of the short-wave instability tells us how the zigzag instability and the short-wave instability interact. Investigations by Waite and Smolarkiewicz into the breakdown of the Lamb-Chaplygin dipole into turbulence and observed that the energy of the zigzag instability grew such that it became the same order of magnitude as the kinetic energy. In these simulations, no short-wave instabilities were observed despite having a similar growth rate. We present results that suggest that the short-wave instability saturates at a level proportional to the aspect ratio δ.

To investigate the saturation level, nonlinear simulations were run with an initially small, $\epsilon = 0.01$, random sinusoidal perturbation of the initial density. Fig. 1.2 is an example of the evolution of the energy for $Re = 5000$ and $F_h = 0.2$. As can be observed in the saturation level occurs at roughly $T = 20$ after which the potential energy states approximately constant. The saturation is defined to be

$$\text{saturation} = \frac{E_{3D}}{E_{2D}} \tag{1.7}$$

where we find the maximum E_{3D} at later times and divide that time by the kinetic energy.

Fig. 1.3 and Fig. 1.4 demonstrate the saturation level for $F_h = 0.2$ and $Re = 2000, 5000$ respectively. The reference line is a slope of 2. In Fig. 1.4 there is some variation in the data points as the length scales get smaller, the definition of when the saturation first occurs is ambiguous. This effect can be observed in Fig. 1.2 as at $T = 30$ the saturation level has increased a little bit from the start of the saturation at $T = 20$. Despite this slight increase, it is clear that the potential energy has saturated.
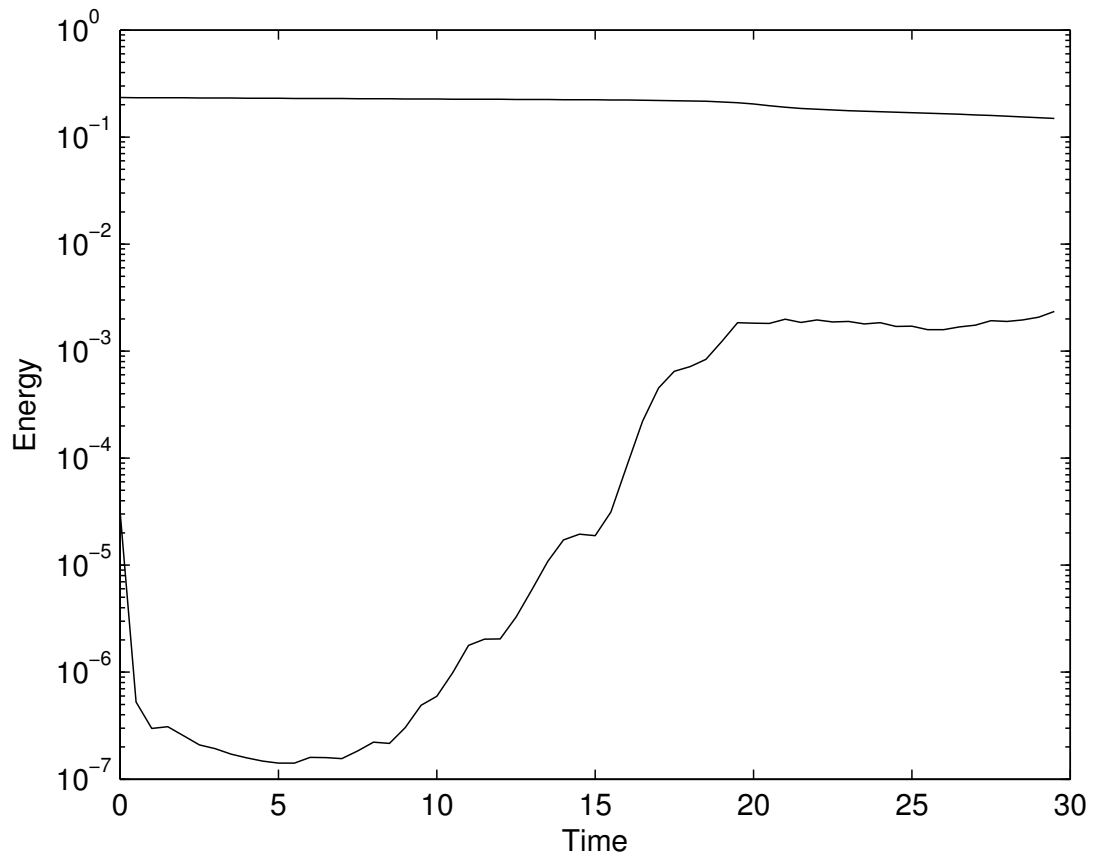
Figure 1.2: Time series of the kinetic energy (top line) and potential energy (bottom line) for $Re = 5000$ and $F_h = 0.2$.
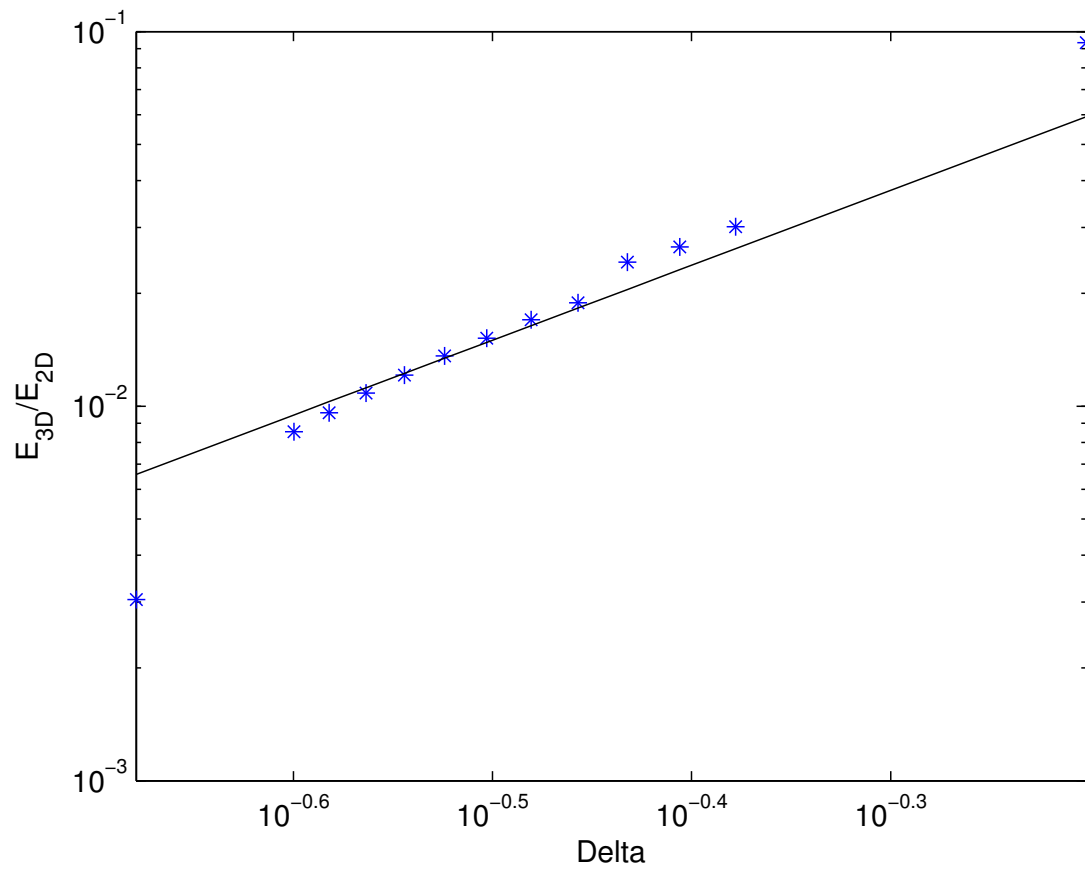
Figure 1.3: Saturation levels for a range of aspect ratios for $Re = 2000$ and $F_h = 0.2$.
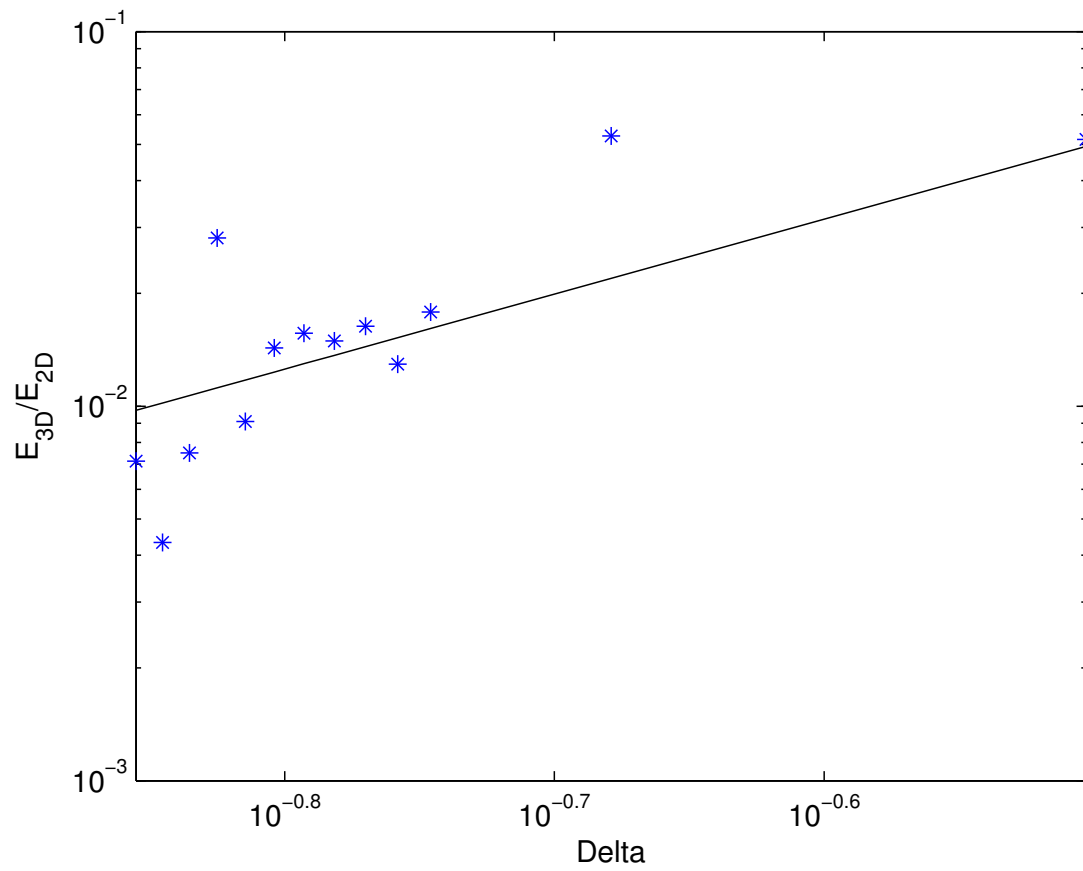
Figure 1.4: Saturation levels for a range of aspect ratios for $Re = 5000$ and $F_h = 0.2$.

The linear fit through these curves suggests that the saturation level depends upon δ as

$$\frac{E_{3Dsat}}{E_{2Dsat}} \sim \delta^2. \tag{1.8}$$

This scaling suggests that as the aspect ratio gets smaller, the saturation level decreases. In Chapter 3, we found that the short-wave instability scaled as $k_z \sim F_h^{-1/5} Re^{2/5}$ thus

$$\frac{E_{3Dsat}}{E_{2Dsat}} \sim \frac{F_h^{2/5}}{H^2 Re^{4/5}}. \tag{1.9}$$

Thus as we increase the Re or horizontal length scale, the saturation level decreases. Alternatively, if we increase stratification, i.e. decrease the Froude number, the saturation level also decreases. Thus, we should not expect the short-wave instability to play a significant role in the evolution of the Lamb-Chaplygin's transition to turbulence.

The scaling suggested has a theoretical backing. In investigations by Ngan, et al [33] into quasi-two dimensional turbulence, they determined that the saturation level of a perturbation depended linearly upon the aspect ratio. We review their derivation. Ngan et. al [33] consider quasi-two dimensional turbulence, which they define to be the three-dimesionalisation of a two-dimensional flow. The study of such flows are motivated by geophysical applications were aspects ratios range from $\delta \sim 0.01 - 0.1$[33].

Ngan et al. now consider a simple scaling analysis [33]. Initially the time scales of the 2D base flow is long compared to that of the 3D base flow. In our results, we verify this. In figure blah note that the time scale of the 2D perturbation, here the top line, is constant while the timescale of the 3D flow is much shorter, which is exemplified by the change that the 3D perturbation goes through over the first 20 or seconds. However once the 3D perturbation saturates, it stops growing and its timescale becomes similar to that of the 2D flow. Now consider the following timescales for these flows [33] as

$$T_{2D} = \frac{U}{L}, \qquad T_{3D} = \frac{u}{H} \tag{1.10}$$

where U is the characteristic velocity of the 2D flow and u is the characteristic velocity. Thus at saturation $T_{2D} \sim T_{3D}$ and thus we have that

$$\frac{U}{L} \sim \frac{u}{H} \Rightarrow \frac{u}{U} \sim \frac{H}{L} = \delta. \tag{1.11}$$

However we are considering the energy and thus we would have to square both sides to get the energy resulting in

$$\frac{E_{2D}}{E_{3D}} \sim \delta^2 \tag{1.12}$$

which is the result suggested by Figs. 1.3 and Fig. 1.4. Thus, the short-wave instability, despite having a similar growth rate to that of the zigzag instability, is saturated at a level proportional to the aspect ratio of the flow, which in stratified flows, is small.

Furthermore, in the scaling analysis derived in the previous chapter, if $\delta < F_h \ll 1$, let us neglect terms of the form F_h/δ, then we would have

$$\frac{\partial \mathbf{u}_h}{\partial t} + \mathbf{u}_h \cdot \nabla_h \mathbf{u}_h + u_z \frac{\partial \mathbf{u}_h}{\partial z} = -\nabla_h p + \frac{1}{Re}\nabla_h^2 \mathbf{u}_h + \frac{1}{\delta^2 Re}\frac{\partial^2 \mathbf{u}_h}{\partial z^2}, \tag{1.13}$$

$$\delta^2 \left(\frac{\partial u_z}{\partial t} + \mathbf{u}_h \cdot \nabla_h u_z + u_z \frac{\partial u_z}{\partial z} \right) = -\frac{\partial p}{\partial z} - \rho' + \frac{\delta^2}{Re}\nabla_h^2 u_z + \frac{1}{Re}\frac{\partial^2 u_z}{\partial z^2}, \tag{1.14}$$

$$\nabla_h \cdot \mathbf{u}_h + \frac{\partial u_z}{\partial z} = 0, \tag{1.15}$$

$$\frac{\partial \rho'}{\partial t} + \mathbf{u}_h \cdot \nabla_h \rho' + u_z \frac{\partial \rho'}{\partial z} - u_z = \frac{1}{ReSc}\nabla_h^2 \rho + \frac{1}{\delta^2 ReSc}\frac{\partial^2 \rho}{\partial z^2}. \tag{1.16}$$

Here stratification has dropped out of the equations of motion and, as discussed, the short-wave instability shouldn't depend on stratification. These equations are very similar to the starting equations of Ngan et al. [33] (+prev paper) which further suggests a link between their derivation and our result. It is important to note, however, that the results of [33] + other are for an inviscid theory. In Fig. 1.1 the saturation level lasts for only a few seconds before the potential energy decreases, most likely due to viscous effects. Regardless, the result is still robust enough that even if the saturation level begins to decrease due to viscosity, its initial maximum is still determined by the aspect ratio.

We conclude with examining the growth rate of the linear theory and that of the nonlinear theory. In comparing the linear theory with the nonlinear theory, there is a problem with what defines the linear regime of the nonlinear simulation. If we examine Fig. 1.2, the growth of the potential energy between $T = 5$ and $T = 20$, it is very difficult to justify approximating this growth rate as linear. For most of the cases of $Re = 5000$ and $F_h = 0.2$, we were unable to determine a consistent way to determine the growth rate of the perturbation and thus we have not included the results for this simulation. Fig. 1.1, which choses a $Re = 2000$ and $F_h = 0.2$ case illustrates the more linear growth rate exhibited by these simulations. Fig. 1.5 illustrates the results for the linear and nonlinear

theories for $Re = 2000$ and $F_h = 0.2$. Here the nonlinear results are greater than those of the linear theory, however the curve still follows the linear theory curve. Again, the issue of the growth in the potential energy not being perfectly linear could contribute to this discrepancy of $8\% - 40\%$.
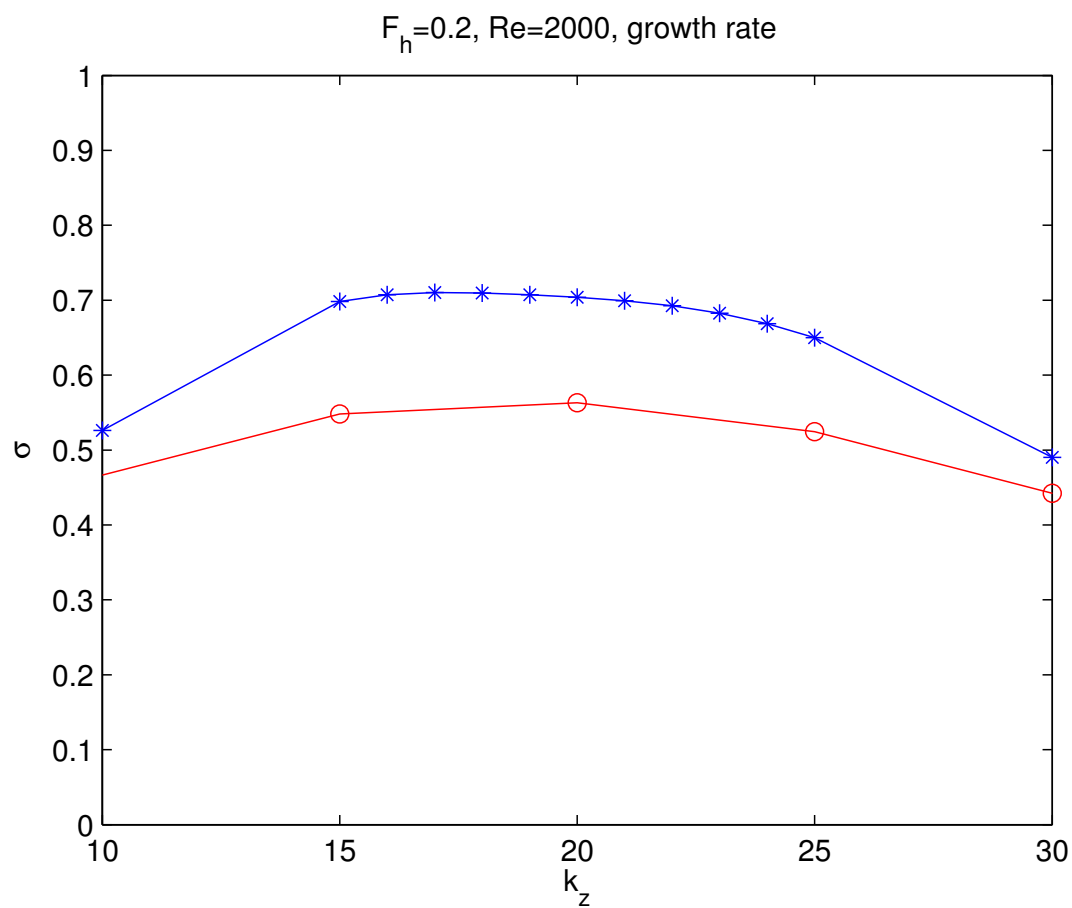
Figure 1.5: Growth rate for $Re = 5000$ and $F_h = 0.2$ with the linear results (red) and the nonlinear results (blue). Note we have not scaled by F_h unlike the results in Chapter 3.

References

[1] David J Acheson. *Elementary fluid dynamics*. Oxford University Press, 1990.

[2] P. Augier and P. Billant. Onset of seconardy instabilities on the zigzag instability in stratified fluids. *J. Fluid Mech*, 682:120–131, 2011.

[3] P. Augier, J.-M. Chomaz, and P. Billant. Spectral analysis of the transition to turbulence from a dipole in stratified fluid. *J. Fluid. Mech*, 713:86–108, 2012.

[4] B.J. Bailey. Three-dimensional instability of elliptical flow. *Phys. Rev. Lett.*, 57:2160, 1986.

[5] G.K. Batchelor. *An Introduction to Fluid Dynamics*. Cambridge University Press, 1967.

[6] P. Billant, P. Brancher, and J.-M. Chomaz. Three-dimensional stability of a vortex pair. *Phys. Fluids*, 11:2069–2077, 1999.

[7] P. Billant and J.-M. Chomaz. Experimental evidence for a new instability of a vertical columnar vortex pair in a strongly stratified fluid. *J. Fluid Mech*, 418:167–188, 2000.

[8] P. Billant and J.-M. Chomaz. Theoretical analysis of the zigzag instability of a vertical columnar vortex pair in a strongly stratified fluid. *J. Fluid Mech*, 419:29–63, 2000.

[9] P. Billant and J.-M. Chomaz. Three-dimensional stability of a vertical columnar vortex pair in a stratified fluid. *J. Fluid Mech*, 419:65–91, 2000.

[10] P. Billant and J.-M. Chomaz. Self-similarity of strongly stratified inviscid flows. *Phys. Fluids*, 13(6):1645–1651, 2001.

[11] L. Bovard and M.L. Waite. Short wave vortex instability in stratified fluids. *Physics of Fluids*, Submitted.

[12] J.P. Boyd. *Chebyshev and Fourier Spectral Methods*. Dover books on mathematics. Dover Publications, 2001.

[13] G. Brethouwer, P. Billant, E. Lindborg, and J.-M. Chomaz. Scaling analysis and simulations of strongly stratified turbulent flows. *J. Fluid Mech*, 585:343–368, 2007.

[14] S.A. Orszag C.M. Bender. *Advanced Mathematical Methods for Scientists and Engineers*. Springer, 1999.

[15] Steven C Crow. Stability theory for a pair of trailing vortices. *AIAA journal*, 8(12):2172–2179, 1970.

[16] A. Deloncle, P. Billant, and J.-M. Chomaz. Nonlinear evolution of the zigzag instability in stratified fluids: a shortcut on the route to dissipation. *J. Fluid Mech*, 660:229–238, 2008.

[17] A. Deloncle, P. Billant, and J.-M. Chomaz. Three-dimensional stability of vortex arrays in a stratified and rotating fluid. *J. Fluid Mech*, 678:482–510, 2011.

[18] P.G. Drazin and W.H. Reid. *Hydrodynamic Instability*. Cambridge University Press, 2004.

[19] Dale R. Durran. *Numerical Methods for Fluid Dyanimcs 2nd Edition*. Springer, 2010.

[20] Matteo Frigo and Steven G Johnson. The design and implementation of fftw3. *Proceedings of the IEEE*, 93(2):216–231, 2005.

[21] D.A. Herbert and S.M. de Bruyn Kops. Predicting turbulence in flows with strong stable stratification. *Phys. Fluids*, 18:18–28, 2006.

[22] R. Kerswell. Elliptical instability. *Annu. Rev. Fluid Mech.*, 34:83–113, 2002.

[23] Kundu. *Fluid Dynamics 5th Edition*. Academic Press, 2012.

[24] M. Lesieur. *Turbulence in Fluids*. Springer, 2008.

[25] T. Leweke and C.H.K. Williamson. Cooperative elliptic instability of a vortex pair. *J. Fluid Mech*, 360:85–119, 1998.

[26] T. Leweke and C.H.K. Williamson. Long-wavelength instability and reconnection of a vortex pair. In E. Krause and K. Gersten, editors, *IUTAM Symposium on Dynamics of Slender Vortices*, volume 44 of *Fluid Mechanics and Its Applications*, pages 225–234. Springer Netherlands, 1998.

[27] D.K. Lilly. Stratified turbulence and the mesoscale variability of the atmosphere. *J. Atmos. Sci*, 40:749, 1983.

[28] E. Lindborg. The energy cascade in a strongly stratified fluid. *J. Fluid Mech*, 550:207–242, 2006.

[29] V.V. Meleshko and G. J. F. van Heijst. On Chaplygin's investigations of two-dimensional vortex structures in an inviscid fluid. *J. Fluid Mech*, 272:157–182, 1994.

[30] C. Meyer. *Matrix Analysis and Applied Linear Algebra Book and Solutions Manual*. Matrix Analysis and Applied Linear Algebra. Society for Industrial and Applied Mathematics, 2000.

[31] T. Miyazaki and Y. Fukumoto. Three-dimensional instability of strained vortices in a stably stratified fluid. *Phys. Fluids A*, 4:2515–2522, 1992.

[32] Saffman PG. Moore DW. The instability of a straight vortex filament in a strain field. *Proc. R. Soc. Lond. A*, 346:413–425, 1975.

[33] K. Ngan, D.N. Straub, and P. Bartello. Aspect ratio effects in quasi-two-dimesional turbulence. *Phys. Fluids*, 17:1–10, 2005.

[34] P. Otheguy, P. Billant, and J.-M. Chomaz. Elliptic and zigzag instabilities on co-rotating vertical vortices in a stratified fluid. *J. Fluid Mech*, 553:253–272, 2006.

[35] Orzag Peterson. Numerical simulation... *collection*, 66614914:1–1000, 1972.

[36] R.T. Pierrehumbert. Universal short-wave instability of two-dimensional eddies in an inviscid fluid. *Phys. Rev. Lett*, 57(17):2157–2159, 1986.

[37] Osborne Reynolds. An experimental investigation of the circumstances which determine whether the motion of water shall be direct or sinuous, and of the law of resistance in parallel channels. *Proceedings of the Royal Society of London*, 35(224-226):84–99, 1883.

[38] J.J. Riley and S. M. de Bruyn Kops. Dynamics of turbulence strongly influenced by buoyancy. *Phys. Fluids*, 15(7):2047–2059, 2003.

[39] J.J. Riley and M.-P. Lelong. Fluid motions in the presence of strong stable stratifications. *Annu. Rev. Fluid Mech.*, 32:613–657, 2000.

[40] J.J. Riley and E. Lindborg. Recent progress in stratified turbulence. In K. Sreenivasan P. Davidson, Y. Kaneda, editor, *Ten Chapters in Turbulence*. Cambridge University Press, 2013.

[41] RD Sharman and MG Wurtele. Ship waves and lee waves. *Journal of the Atmospheric Sciences*, 40:396–427, 1983.

[42] Lloyd N. Trefethen. *Spectral Methods in MATLAB*. SIAM, 2000.

[43] D.J. Tritton. *Physical Fluid Dynamics*. Oxford Science Publications. Clarendon Press, 1988.

[44] Widnall SE Tsai C-Y. The stability of short waves on a straight vortex filament in a weak externally imposed strain field. *J. FLuid Mech*, 73:721–733, 1976.

[45] G.K. Vallis. *Atmospheric and Oceanic Fluid Dynamics: Fundamentals and Large-scale Circulation*. Cambridge University Press, 2006.

[46] Milton Van Dyke. *Perturbation Methods in Fluid Mechanics*. Parabolic Press Stanford, 1975.

[47] Milton Van Dyke. *An Album of Fluid Motion*. Parabolic Press Stanford, 1982.

[48] M.L. Waite. Stratified turbulence at the buoyancy scale. *Phys. Fluids*, 23:23–35, 2012.

[49] M.L. Waite and P. Bartello. Stratified turbulence dominated by vortical motion. *J. Fluid Mech*, 517:281–301, 2004.

[50] M.L. Waite and P.K. Smolarkiewicz. Instabilty and breakdown of a vertical vortex pair in a strongly stratified fluid. *J. Fluid Mech.*, 606:239–273, 2008.

[51] R.M. Wald. *General Relativity*. University of Chicago Press, 2010.

[52] F. Waleffe. On the three-dimensional instability of strained vortices. *Phys. Fluids A*, 3:76, 1990.

[53] S.E. Widnall, D.B. Bliss, and C.Y. Tsai. The instability of short waves on a vortex ring. *J. Fluid Mech*, 66:35, 1974.